Time Courses of Cortical Glucose Metabolism and Microglial Activity Across the Life Span of Wild-Type Mice: A PET Study

Matthias Brendel*[1], Carola Focke*[1], Tanja Blume[1,2], Finn Peters[2], Maximilian Deussing[1], Federico Probst[1], Anna Jaworska[2,3], Felix Overhoff[1], Nathalie Albert[1], Simon Lindner[1], Barbara von Ungern-Sternberg[1], Peter Bartenstein[1], Christian Haass[4–6], Gernot Kleinberger[4,5], Jochen Herms[2,5,6], and Axel Rominger[1,5]

[1]Department of Nuclear Medicine, University of Munich, Munich, Germany; [2]Center for Neuropathology and Prion Research, Ludwig-Maximilians-Universität München, Munich, Germany; [3]Laboratory of Neurodegeneration, International Institute of Molecular and Cell Biology, Warsaw, Poland; [4]Biomedical Center (BMC), Biochemistry, Ludwig-Maximilians-Universität München, Munich, Germany; [5]Munich Cluster for Systems Neurology (SyNergy), Munich, Germany; and [6]DZNE—German Center for Neurodegenerative Diseases, Munich, Germany

Contrary to findings in the human brain, ^{18}F-FDG PET shows cerebral hypermetabolism of aged wild-type (WT) mice relative to younger animals, supposedly due to microglial activation. Therefore, we used dual-tracer small-animal PET to examine directly the link between neuroinflammation and hypermetabolism in aged mice. **Methods:** WT mice (5–20 mo) were investigated in a cross-sectional design using ^{18}F-FDG (n = 43) and translocator protein (TSPO) (^{18}F-GE180; n = 58) small-animal PET, with volume-of-interest and voxelwise analyses. Biochemical analysis of plasma cytokine levels and immunohistochemical confirmation of microglial activity were also performed. **Results:** Age-dependent cortical hypermetabolism in WT mice relative to young animals aged 5 mo peaked at 14.5 mo (+16%, $P < 0.001$) and declined to baseline at 20 mo. Similarly, cortical TSPO binding increased to a maximum at 14.5 mo (+15%, $P < 0.001$) and remained high to 20 mo, resulting in an overall correlation between ^{18}F-FDG uptake and TSPO binding (R = 0.69, $P < 0.005$). Biochemical and immunohistochemical analyses confirmed the TSPO small-animal PET findings. **Conclusion:** Age-dependent neuroinflammation is associated with the controversial observation of cerebral hypermetabolism in aging WT mice.

Key Words: TSPO PET; FDG PET; hypermetabolism; aging; wild-type mice

J Nucl Med 2017; 58:1984–1990
DOI: 10.2967/jnumed.117.195107

Small-animal PET in transgenic mouse models of Alzheimer disease (AD) is a promising technique for monitoring disease-modifying treatments in vivo (*1*). Clinical PET imaging with the glucose analog ^{18}F-FDG has become a standard procedure for detecting defects in cerebral glucose metabolism characteristic of AD and other brain diseases (*2–4*).

Although confirmation of advanced AD by ^{18}F-FDG PET is unproblematic, preclinical stages of AD manifest in only subtle deviations from the cerebral metabolism typical of the healthy brain. Furthermore, cerebral atrophy and relative hypometabolism both occur in healthy aging, notably in medial frontal regions (*5–7*) such that age-dependent templates are needed for voxelwise comparisons of ^{18}F-FDG PET (*8*). In contrast to the established findings of age-related hypometabolism in the healthy human brain, previous preclinical studies found glucose hypermetabolism in aged wild-type (WT) mice relative to younger animals (*9,10*). Microglial activation has been suggested as a possible driver for age-related ^{18}F-FDG hypermetabolism in mice (*11*). To test this hypothesis, we earlier undertook a dual-tracer small-animal PET study with ^{18}F-FDG and also ^{18}F-GE180, a tracer for the 18-kDa translocator protein (TSPO), which is highly expressed at the outer mitochondrial membrane of activated microglia; preliminary results indicated an association between aged-dependent parallel increases in TSPO binding and ^{18}F-FDG uptake in a transgenic AD model and also WT mice (*12*). To better characterize this association, we have obtained ^{18}F-GE180 and ^{18}F-FDG small-animal PET recordings in a large series of C57BL/6 WT mice of various ages in a study of cross-sectional design. We predicted that there should be parallel age-dependent increases of both biomarkers, with regional colocalization of the increases in tracer uptake. Finally, we aimed to test whether neuroinflammation and glucose hypermetabolism correlate in individual mice, and also undertook additional biochemical analyses of inflammatory cytokines in brain and immunohistochemical analysis of microglial activation to cross-validate the small-animal PET results.

MATERIALS AND METHODS

Animals and Study Design

All experiments were performed in compliance with the National Guidelines for Animal Protection, Germany, and with the approval of the regional animal care committee (Regierung Oberbayern), and were overseen by a veterinarian. Animals were housed in a temperature- and humidity-controlled environment with a 12-h light–dark cycle, with free access to food (Ssniff) and water. All studies were performed in female WT C57BL/6 mice aged 5–20 mo, purchased from Charles River.

Received Apr. 24, 2017; revision accepted Jun. 9, 2017.
For correspondence or reprints contact: Axel Rominger, Marchioninistrasse 15, Department of Nuclear Medicine, University of Munich, Munich, Germany.
E-mail: axel.rominger@med.uni-muenchen.de
*Contributed equally to this work.
Published online Jul. 13, 2017.

Small-animal PET examinations were performed in a cross-sectional design for glucose metabolism ($n = 43$) and TSPO ($n = 58$). In particular, a subset of 8 mice aged 8 and 14.5 mo received both tracer examinations within a span of 1 wk, so as to test directly for correlation of the 2 markers in individual mice. Another subset of mice ($n = 7$ for glucose metabolism and $n = 8$ for TSPO) underwent between 2 and 4 small-animal PET investigations with each tracer (true longitudinal setting). All other mice were examined once with either ^{18}F-FDG or TSPO PET.

Subsets of mice in the youngest and oldest groups were killed after scanning, followed by rapid brain removal and performance of enzyme-linked immunosorbent assay for inflammatory cytokine levels in brain extracts, and also immunohistochemistry analyses. Group sizes by age and type of measurement are presented in Table 1.

Radiochemistry

Radiosynthesis of ^{18}F-GE180 was performed as previously described (*13*), with slight modifications (*12*). This procedure yielded a radiochemical purity exceeding 98% and a specific activity of 1,400 ± 500 GBq/μmol at the end of synthesis. ^{18}F-FDG was purchased commercially.

Small-Animal PET Data Acquisition and Reconstruction

All mice were anesthetized with isoflurane (1.5%, delivered at 3.5 L/min) and placed in the aperture of the Siemens Inveon DPET, as described previously (*14*). Further details are provided in the supplemental materials (available at http://jnm.snmjournals.org).

Small-Animal PET Data Analyses

All single-frame static datasets (30–60 min or 60–90 min) were coregistered to an MRI mouse atlas (*15*) by a manual rigid-body transformation using the PMOD fusion tool (version 3.5; PMOD Technologies Ltd.) after the mouse identity was anonymized to the reader. Accurate initial alignment was verified by a second experienced reader. In the second step, a reader-independent, fine coregistration to tracer-specific templates was performed (*16*). These templates had been generated by averaging all available age-specific PET scans of a single tracer after minor spatial reregistrations to ensure optimal overlapping. Here, the initial manual small-animal PET–to–MRI atlas fusion images were spatially normalized to the tracer-specific templates by a nonlinear brain normalization tool in PMOD (equal modality; smoothing by 0.6 mm; nonlinear warping; 16 iterations; frequency cutoff, 3; regularization, 1.0; no thresholding).

TABLE 1
Study Overview

Age (mo)	PET, ^{18}F-GE180 (*n*)	PET, ^{18}F-FDG (*n*)	ELISA, IL1b, IL6, KC/GRO (*n*)	Immunohistochemistry, Iba1 (*n*)
5–6	8	9	6	5
8	19	9		
13	7			
14.5	9	10		
16	7	11		
19–20	8	4	6	5

Dual small-animal PET experiments, enzyme-linked immunosorbent assay (ELISA), and immunohistochemistry were performed in groups of WT C57BL/6 mice at various ages.

The concatenation of both transformations was then applied to small-animal PET images in the native space, so as to obtain optimal resampling with a minimum of interpolation.

A bilateral frontal cortical target volume of interest (VOI; comprising 24 mm^3 in total) was used for both tracers. The bilateral striatum VOI (21 mm^3) was applied as a representative forebrain region with low TSPO density. Bilateral hippocampal (comprising 10 mm^3 in total) and parietal (comprising 14 mm^3 in total) VOIs were used for extended analyses. The previously validated oval-shaped reference tissue VOI containing white matter of the cerebellum and the brain stem (comprising 29 mm (*3,12*)) was used for SUV normalization of ^{18}F-GE180 small-animal PET images. On the basis of our previous experience, the entire cerebellum (comprising 65 mm^3) was used for scaling of ^{18}F-FDG data. Target–to–reference tissue SUV ratios (SUVRs) were calculated for ^{18}F-GE180 and ^{18}F-FDG.

Statistical Parametric Mapping (SPM) Analysis and Dice Coefficient

For both tracers, whole-brain voxelwise comparisons between young (5–6 mo) and moderately aged (14.5 mo) WT mice were performed by SPM using SPM5 routines (Wellcome Department of Cognitive Neurology, University College London) implemented in MATLAB (version 7.1), as adapted from Sawiak et al. (*17*) for mouse data. Both age groups were selected after completion of the VOI-based analysis because they represented the maximum age-dependent increase for both tracers. T-score maps of the age group contrasts were all corrected for multiple comparisons (false-discovery rate [FDR]–corrected) at a significance level of P less than 0.05. Significant areas were binarized by the respective T-score threshold for each tracer and used to define the overlap of regions with specific increases in tracer uptake with age.

The Sørensen–Dice index for comparing the similarity of 2 samples (*18*) was calculated for the T-statistic maps of longitudinal ^{18}F-GE180 and ^{18}F-FDG uptake differences (14.5 mo > 5–6 mo) to assess the spatial agreement of the pseudolongitudinal binding increases with age.

Details about immunohistochemistry (acquisition and image analysis) as well as biochemical analyses of cytokines are provided in the supplemental materials.

Statistics

Statistical analyses of PET data were performed in SPSS (version 23; SPSS Software, IBM). Group comparisons of VOI-based small-animal PET results between different age groups were assessed by ANOVA with Tukey post hoc correction. For correlation analyses, Pearson coefficients of correlation (R) were calculated. Multiple regression analysis was performed to investigate the association of cortical glucose metabolism and microglial activation with age as a fixed effect. The standardized regression coefficients (β) are reported. Statistics of histologic and volumetric analyses were calculated in Prism (version 5.04; GraphPad Software). An analysis of the difference in the volumes of cortex and motor cortex between aged and young mice was performed using an unpaired Student t test. Other intergroup comparisons were performed using the 2-tailed Student t test. The Kolmogorov–Smirnov test (KS test) was used to confirm the statistical results based on the Student t test. The KS test enables determination of whether 2 datasets differ significantly, based on statistics that measure the greatest distance between the empiric distribution function of the univariate dataset and the comparison step function of the second dataset. Here, we compared the fraction of different somal volumes of microglia between young and aged mice.

For all comparisons, a threshold of P less than 0.05 was considered to be significant for rejection of the null hypothesis.

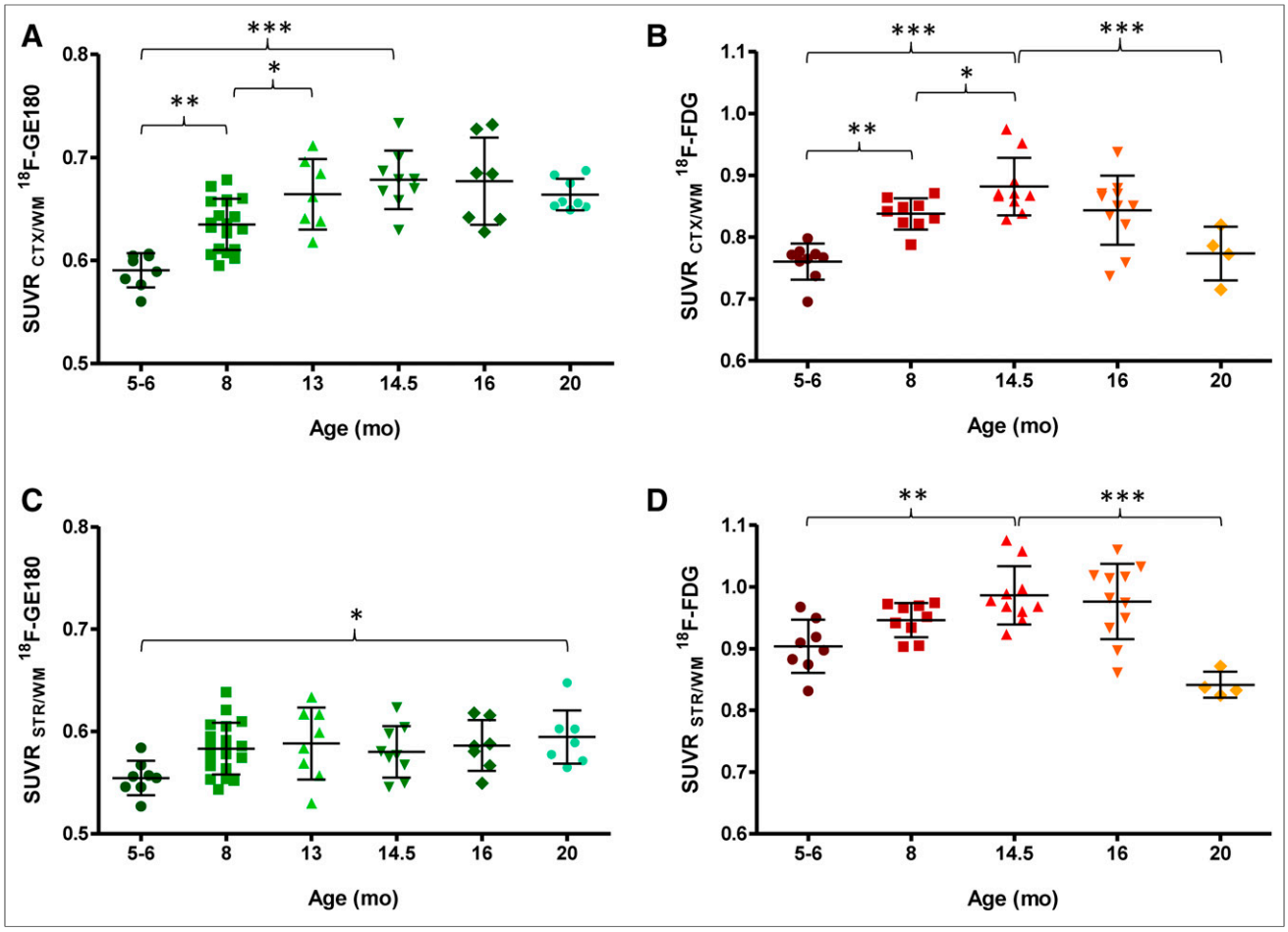

FIGURE 1. Plots show mean (±SD) cortical SUVR of ^{18}F-GE180 (A) and ^{18}F-FDG (B) in C57BL/6 mice at different ages. Corresponding striatal SUVRs are provided in C and D. Significant differences between subgroups are marked by $^{*}P < 0.05$, $^{**}P < 0.01$, $^{***}P < 0.001$; ANOVA with Tukey post hoc correction.

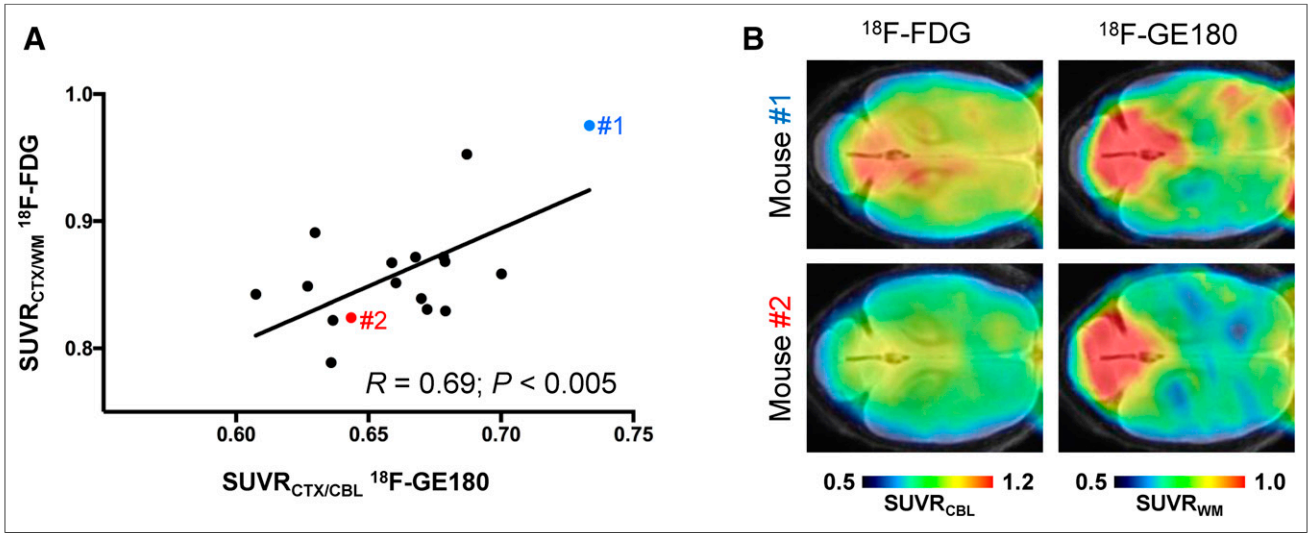

FIGURE 2. (A) Correlation analysis between cortical TSPO binding and glucose metabolism in a subset of C57BL/6 mice ($n = 16$) in which both PET measurements were conducted within the same week. Images from 2 representative mice aged 14.5 mo are illustrated as horizontal slices through neocortex coregistered with T1 MRI template (red and blue circles in plot). (B) Mouse 1 indicated high cortical glucose metabolism and high TSPO binding, whereas mouse 2 had comparably low cortical glucose metabolism and low TSPO binding.

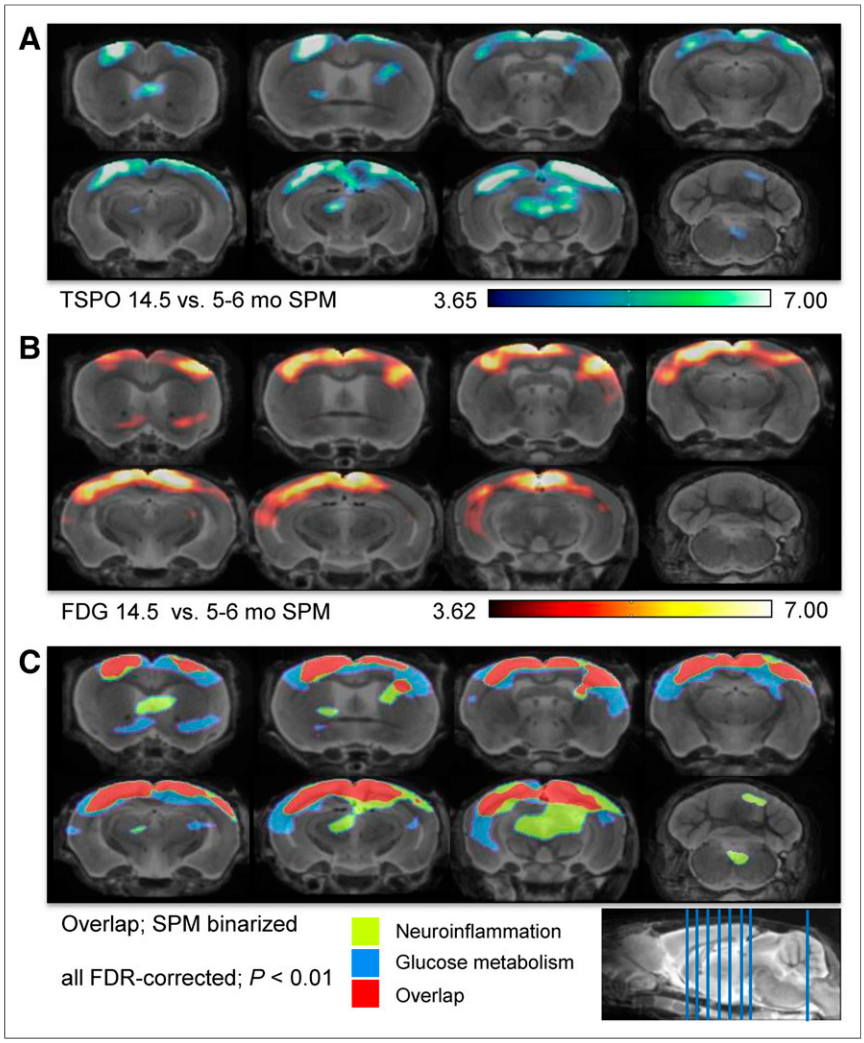

FIGURE 3. Voxelwise regional increases of radiotracer uptake in aged compared with young C57BL/6 mice for TSPO binding (A) and glucose metabolism (B) as assessed by SPM. (C) Binarized specific increases in ^{18}F-GE180 uptake, indicating microglial activation (green); binarized specific increases in ^{18}F-FDG uptake, indicating hypermetabolism (blue); and areas of overlapping increases for both tracers (red) are projected on coronal slices of MRI mouse atlas, as depicted in planes on midsagittal slice. All $P < 0.01$, FDR-corrected.

RESULTS

Dual-Tracer Small-Animal PET Analyses

For both tracers, a significant cortical increase was already observed between 5- to 6-mo-old and 8-mo-old C57BL/6 mice (^{18}F-FDG, +10%, $P < 0.005$; ^{18}F-GE180, +8%, $P < 0.005$; Figs. 1A and 1B). C57BL/6 mice (14.5 mo old) indicated parallel cortical increases for glucose metabolism and TSPO binding compared with 5- to 6-mo-old animals (^{18}F-FDG, +16%, $P < 0.001$; ^{18}F-GE180, +15%, $P < 0.001$). In the most aged mice (≥14.5 mo), there was a slowly descending plateau for the TSPO SUVR, whereas ^{18}F-FDG uptake declined from a peak to that seen in the youngest group (20 vs. 14.5 mo: −12%, $P < 0.001$). Findings of longitudinal imaging were congruent with cross-sectional data (Supplemental Fig. 2).

Striatal TSPO binding increased nonsignificantly from 5–6 to 8 mo of age (+5%), and the only significant difference was observed in the contrast between 5–6 and 20 mo (+7%, $P < 0.05$; Fig. 1C). Glucose metabolism in the striatum increased with age, peaking at 14.5 mo (14.5 vs. 5–6 mo, +9%, $P < 0.01$) and then dropping below the baseline level at the age of 20 mo (20 vs. 5–6 mo, −7%, P = not significant; 20 vs. 16 mo, −14%, $P < 0.01$; Fig. 1D). Hippocampal and parietal findings of TSPO binding and glucose metabolism are provided Supplemental Figure 3.

Correlation Analyses of PET Studies

In a subset of C57BL/6 mice (8 and 14.5 mo; $n = 8$ each) both small-animal PET measurements were conducted within the same week. In these mice, the cortical SUVR results for ^{18}F-FDG and ^{18}F-GE180 correlated within individual mice ($R = 0.69$, $P < 0.005$; Fig. 2). We next inquired whether cortical glucose metabolism is associated with TSPO binding independently of age. To this end, we performed a multiple-regression analysis with ^{18}F-FDG SUVR as an outcome variable, with ^{18}F-GE180 SUVR as predictor, and with introduction of age as a covariate. In this analysis, cortical ^{18}F-FDG SUVR was significantly associated with cortical ^{18}F-GE180 SUVR ($\beta = 0.61$; $P < 0.05$), after adjusting for age. Striatal uptake of the 2 tracers did not correlate with each other ($R = 0.06$, P = not significant).

Voxelwise Analyses of PET Studies

SPM indicated a clear spatial relationship between age-dependent alterations of neuroinflammation and glucose metabolism as measured in vivo by small-animal PET. C57BL/6 mice revealed a cortically pronounced increase of TSPO binding (Fig. 3A) and glucose metabolism (Fig. 3B) between 5–6 and 14.5 mo. In particular, the longitudinal increases of both tracers exceeding the threshold for FDR correction ($P < 0.01$) overlapped in 36 mm^3 of the entire neocortical brain volume (primary and secondary motor areas, primary somatosensory areas, anterior cingulate cortex, Fig. 3C). Glucose metabolism comprised additional longitudinal increases in a further 37 mm^3 of the brain volume, encompassing mostly lateral cortical areas and minor clusters in subcortical areas (thalamus, striatum). A larger volume showed a specific increase of ^{18}F-GE180 signal without elevated ^{18}F-FDG uptake (68 mm^3; predominantly subcortical areas: midbrain, thalamus, striatum). The calculated Sørensen–Dice coefficient confirmed a high similarity of 54.5% between the parametric age-dependent increase maps of ^{18}F-GE180 and ^{18}F-FDG.

Immunohistochemistry and 3-Dimensional Volumetric Analyses

We confirmed the immunohistochemical correlates of increasing TSPO binding evident to ^{18}F-GE180 small-animal PET in older WT mice. The volume percentage of Iba1-positive microglial soma was significantly elevated in aged WT mice when compared with the young cohort (0.44% ± 0.03% vs. 0.33% ± 0.02%; $P < 0.05$; Fig. 4A), whereas volume percentage of

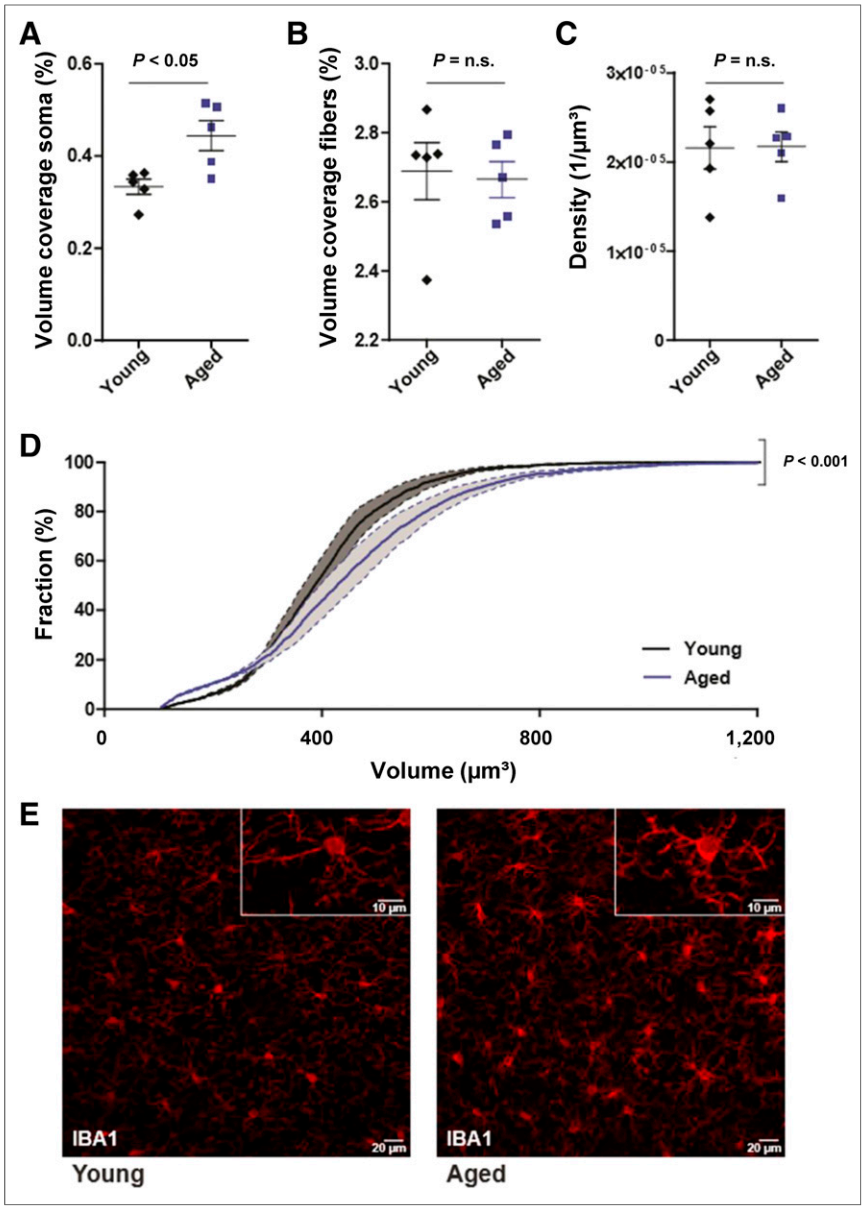

FIGURE 4. Quantification of volume coverage of soma (A) and fibers (B) of Iba1-positive microglia showed increase in somal volume in aged (19–20 mo old) WT mice, whereas no change in fiber volumes could be observed. (C) Quantification of microglial density showed no difference between young and aged mice. (D) Cumulative sum of somal volumes indicates shift toward larger volumes in aged mice. (E) Confocal images of Iba1 immunostainings in young and aged mouse cortex. Data are mean ± SEM, $n = 5$ per group, 2-tailed Student t test. n.s. = not significant.

Iba1-positive fibers did not reveal a significant difference (2.66% ± 0.05% vs. 2.68% ± 0.08%; P = not significant; Fig. 4B). The density of Iba1-positive microglial cells was equal between aged and young WT mice (2.2 vs. 2.2E^{-5}/µm^3; P = not significant; Fig. 4C). By plotting all analyzed somal volumes against their frequency, we identified a clear shift toward larger volumes for aged WT mice (Fig. 4D). Indeed, larger somal volumes in aged WT mice were discernible to visual inspection of the micrographs (compare young and aged in Fig. 4E). Three-dimensional volumetric analyses revealed identical cortical volumes for young and aged mice (29.0 ± 1.8 vs. 28.3 ± 1.6 mm^3, P = not significant; Supplemental Fig. 4).

Enzyme-Linked Immunosorbent Assay

Biochemical analysis of WT brains confirmed an age-dependent neuroinflammation as indicated by elevated cytokines at 19–20 mo compared with 6 mo: IL-1 (+63%; $P < 0.05$; Fig. 5A), IL-6 (+23%; $P < 0.005$; Fig. 5B), and KC/GRO (+91%; $P < 0.05$; Fig. 5C).

DISCUSSION

To our knowledge, this is the first large-scale in vivo study aiming to uncover molecular and cellular relationships between glucose metabolism and microglial activation during aging of WT mice. We performed dual in vivo small-animal PET with the novel TSPO tracer ^{18}F-GE180 and the commonly used glucose metabolism tracer ^{18}F-FDG in WT mice in conjunction with biochemical assessments of neuroinflammatory markers. This analysis revealed close temporal and spatial correlations between the age-dependent increases of both small-animal PET biomarkers. Immunohistochemical and biochemical assessments confirmed the TSPO small-animal PET findings, thus providing consistent evidence that the previously described cortical hypermetabolism in aged WT mice is accompanied by increasing neuroinflammation. These preclinical findings substantiate a contribution of microglial activation in aging WT mice to the net energy balance of brain.

As in previous small-animal PET studies (*9,10,12*), we found an increase of ^{18}F-FDG uptake in the cortex of WT mice between 5–6 and 14.5 mo of age. To date, the reason for this discrepancy with the age-related decrease of ^{18}F-FDG metabolism in the human cerebral cortex (*5–7*) has been a matter of speculation. Our in vivo findings in WT C57BL/6 mice show a clear temporal and spatial association between neuroinflammation to TSPO small-animal PET and cortical glucose metabolism, likewise assessed by small-animal PET. The present finding of age-related increased cortical TSPO signal is strongly supported by a recent study (*19*), which also reported an age-dependent increase of ^{18}F-GE180 uptake in WT mice from 4 to 26 mo in vivo, as confirmed by ex vivo autoradiography. Our in vivo finding of increased neuroinflammation in aged WT mice was confirmed by postmortem assessments of elevated immunostaining of microglial cells and proinflammatory cytokine levels in the brains of aged mice. Interestingly, the microglial cell and Iba1-positive fiber densities were unchanged, but the diameter of microglial soma was higher in the aged mice (Fig. 4). These findings are in line with an earlier report on microglia in C57BL/6J-Iba1-eGFP mice, in which the authors found increasing somal diameter and decreasing microglial filament length in older mice (*20*). We note that the age of our

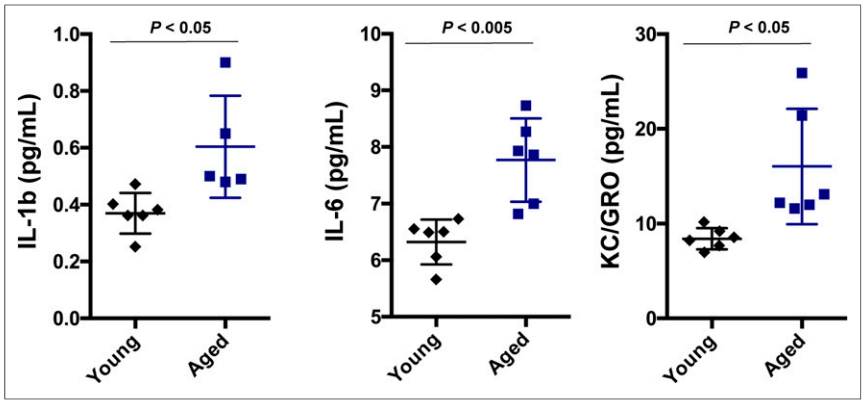

FIGURE 5. Summary of cytokine findings in WT mice aged 6 and 19–20 mo. Bar graphs show mean ± SD for IL-1b, IL-6, and keratinocyte chemoattractant (KC)/human growth–regulated oncogene (GRO) chemokine levels.

oldest mice (19–20 mo) fell midway between the adult (11–12 mo) and aged (26–27 mo) groups of their study. Importantly, increased somal volume is an index of higher activation states of microglia (*21*). Although our TSPO immuinohistochemical staining did not afford quantitation of off-target binding in vessels, it clearly indicated a colocalization of TSPO positivity in microglial soma and only sparse staining in fibers (Supplemental Fig. 5).

This dissociation between soma and ramifications is unsurprising, because TSPO is localized at the outer membrane of mitochondria (*22*), which are mainly confined to the cell bodies, sparsely present in thick dendrites and nearly absent from distal dendrites. Although we did not directly test this link with organelles, it seems plausible that enlarged soma of activated microglial aged mice should contain more mitochondria, which together probably contribute to elevated TSPO activity and glucose consumption. Microglia, as the resident macrophages of the brain are a highly mobile cell population (*23*) and are highly dependent on glucose, and to a lesser extent on fatty acids for energy metabolism (*24*). At present, the contribution of microglia to the cortical energy budget is unknown; this might be ascertainable by high-resolution electron microscopy in conjunction with ^{3}H2-deoxyglucose autoradiography, as in early studies of cellular metabolism in invertebrate ganglia (*25*). However, it seems certain that microglial activation as occurs in aging WT mice may become a significant component of the brain total energy budget.

It remains uncertain why the trajectories of cortical glucose metabolism with age differ in the rodent and human brains. Human postmortem data have revealed larger somal volumes and more proinflammatory transcripts in senescent microglia (*26*), thus matching the phenotype in the present study. Interestingly, microglial activation in the aged human brain makes the hippocampus more vulnerable to cognitive decline (*27*). Additionally, senescent microglia are primed to be more reactive to inflammatory stimuli, thus tending to overproduce proinflammatory cytokines for an extended period, which results in maladaptive sickness responses (*28*). Importantly, not only general markers of neuroinflammation but also specifically TSPO binding have been shown to increase during healthy human aging (*29*). In accord with that observation, we see increasing TSPO signal during normal aging in WT mice, which seemingly reaches a plateau at 20 mo of age. Interestingly, the largest step in increase of TSPO (and ^{18}F-FDG) signal was observed between young mice at 5–6 mo and 8 mo of age, which is rather precipitous in this brief interval. We can only speculate about the reason for this transition, which may be related to environmental stresses arising from transfer from the breeding laboratory to our facility (*30*).

The well-known cortical hypometabolism of healthy aged humans (*7*) was distinctly absent in aging WT mice. This disagreement might arise from the different life expectancy of mice and humans; the declining cerebral energy metabolism is first evident in the human brain by the age of 50 y (*7*), which is mirrored by declines in oxygen extraction fraction (*31*). Middle age for humans might be compared with an age of 16 mo in mice (*32*). Indeed, present data indicated a plateau after 14.5 mo of age for cortical ^{18}F-GE180 binding, whereas the peak in ^{18}F-FDG uptake is followed at 20 mo by a significant decrease to levels typical of young mice (Fig. 1). Insofar as ^{18}F-FDG uptake is most likely the composite of normal neuronal and astroglial glucose metabolism (*33*) plus inflammation-related microglial activation, we interpret the age-dependency to reflect the sum of the 3 cellular components, each with its own trajectory. The evident uncoupling of glucose metabolism and microglial activity in mice aged older than 14.5 mo is potentially related to the onset of age-dependent neurodegeneration, such that neuronal metabolism becomes the driver for net changes in glucose consumption in aged mice. Indeed, striatal glucose metabolism at 20 mo had decreased to even below the 5- to 6-mo baseline data, which supports the above interpretation, as the microglial proportion of the ^{18}F-FDG signal is likely lower for this region (compare regional TSPO activity in Figs. 1C and 1A). Thus, the striatal glucose metabolism probably decreases due to age-dependent neurodegeneration, which is not masked by increasing microglial glucose consumption. It needs to be elucidated in future studies whether there is a causal relationship between early cortical microglial activation and later decreases in glucose metabolism of the entire forebrain. Our findings predict a further decrease of cortical glucose metabolism in very aged mice (>20 mo). However, because of the increasing dropout rates, we decided to confine our investigation to a younger age range, which is typical for most of the earlier small-animal PET studies.

At least in human neurodegenerative disease, there is an inverse relationship between cortical TSPO binding and ^{18}F-FDG uptake (*34*). However, PET studies do not distinguish the cellular site of TSPO binding or metabolism; another investigation suggests that glucose consumption of inflammatory cells could mask the true extent of specifically neuronal metabolism deficits in the aging brain (*11*). In regional analysis of our WT mice, we confirmed a high spatial similarity by the calculated Sørensen–Dice coefficient (54.5%), which fits to the proposed colocalization of the increases in the 2 markers. This conclusion has implications for our previous findings in a transgenic PS2APP AD mouse model with known cognitive decline despite elevated cortical glucose metabolism (*12*). In light of the current findings, the elevated glucose metabolism in that study was likely driven by the pronounced microglial response, which would have masked a decrease of neuronal glucose consumption. As noted above, electron microscopy in conjunction with ^{3}H2-deoxyglucose autoradiography could resolve the microglial contribution to the brain energy budget.

The study has several limitations. Global changes in ^{18}F-FDG uptake during healthy aging of mice are possibly missed as they

would be masked by the reference region scaling of the applied SUVR method; absolute quantitation of the cerebral metabolic rate for glucose relative to an image-derived input function (*35*) might give a clearer depiction of age-related changes. Regional cerebral blood flow is known to influence (semiquantitative) assessments of glucose metabolism using the current SUVR method (*36*), such that age-dependent perfusion changes may be a confounder in our ^{18}F-FDG analyses. Nonetheless, SUVR methods are standard practice in clinical ^{18}F-FDG PET imaging (*37*), which may justify the design of the present preclinical study. A true longitudinal setting might be preferable to the present cross-sectional design, but would have entailed as many as 10 small-animal PET examinations for each biomarker in each mouse; this would be logistically difficult because of the incidence of dropouts.

CONCLUSION

We demonstrated an age-dependent and highly colocalized increase of cortical glucose metabolism to ^{18}F-FDG and TSPO binding to ^{18}F-GE180 small-animal PET in WT mice aged from 5 to 14.5 mo. Age-dependent cortical neuroinflammation potentially explains the widely described but controversially discussed hypermetabolism in aged C57/BL6 mice. The contribution of activated microglia to the brain energy budget should be considered in ^{18}F-FDG PET studies of AD and other neuroinflammatory conditions. Furthermore, present findings emphasize the need for age-matched controls in preclinical research of TSPO activity and glucose metabolism.

DISCLOSURE

The study was financially supported by the SyNergy Cluster (Jochen Herms, Peter Bartenstein, Christian Haass, and Axel Rominger). No other potential conflict of interest relevant to this article was reported.

ACKNOWLEDGMENTS

Manuscript editing was provided by Inglewood Biomedical Editing. GE180 cassettes were purchased from GE Healthcare.

REFERENCES

1. Brendel M, Jaworska A, Herms J, et al. Amyloid-PET predicts inhibition of de novo plaque formation upon chronic gamma-secretase modulator treatment. *Mol Psychiatry.* 2015;20:1179–1187.
2. Bohnen NI, Djang DS, Herholz K, Anzai Y, Minoshima S. Effectiveness and safety of ^{18}F-FDG PET in the evaluation of dementia: a review of the recent literature. *J Nucl Med.* 2012;53:59–71.
3. Minoshima S, Frey KA, Koeppe RA, Foster NL, Kuhl DE. A diagnostic approach in Alzheimer's disease using three-dimensional stereotactic surface projections of fluorine-18-FDG PET. *J Nucl Med.* 1995;36:1238–1248.
4. Tripathi M, Tripathi M, Damle N, et al. Differential diagnosis of neurodegenerative dementias using metabolic phenotypes on F-18 FDG PET/CT. *Neuroradiol J.* 2014;27:13–21.
5. Hsieh TC, Lin WY, Ding HJ, et al. Sex- and age-related differences in brain FDG metabolism of healthy adults: an SPM analysis. *J Neuroimaging.* 2012;22:21–27.
6. Yoshizawa H, Gazes Y, Stern Y, Miyata Y, Uchiyama S. Characterizing the normative profile of ^{18}F-FDG PET brain imaging: sex difference, aging effect, and cognitive reserve. *Psychiatry Res.* 2014;221:78–85.
7. Kakimoto A, Ito S, Okada H, Nishizawa S, Minoshima S, Ouchi Y. Age-related sex-specific changes in brain metabolism and morphology. *J Nucl Med.* 2016;57:221–225.
8. Ishii K, Willoch F, Minoshima S, et al. Statistical brain mapping of ^{18}F-FDG PET in Alzheimer's disease: validation of anatomic standardization for atrophied brains. *J Nucl Med.* 2001;42:548–557.
9. de Cristóbal J, Garcia-Garcia L, Delgado M, Perez M, Pozo MA, Medina M. Longitudinal assessment of a transgenic animal model of tauopathy by FDG-PET imaging. *J Alzheimers Dis.* 2014;40(suppl 1):S79–S89.
10. Poisnel G, Herard AS, El Tannir El Tayara N, et al. Increased regional cerebral glucose uptake in an APP/PS1 model of Alzheimer's disease. *Neurobiol Aging.* 2012;33:1995–2005.
11. Backes H, Walberer M, Ladwig A, et al. Glucose consumption of inflammatory cells masks metabolic deficits in the brain. *Neuroimage.* 2016;128:54–62.
12. Brendel M, Probst F, Jaworska A, et al. Glial activation and glucose metabolism in a transgenic amyloid mouse model: a triple-tracer PET study. *J Nucl Med.* 2016;57:954–960.
13. Wickstrøm T, Clarke A, Gausemel I, et al. The development of an automated and GMP compliant FASTlab synthesis of [^{18}F]GE-180; a radiotracer for imaging translocator protein (TSPO). *J Labelled Comp Radiopharm.* 2014;57:42–48.
14. Rominger A, Mille E, Zhang S, et al. Validation of the octamouse for simultaneous ^{18}F-fallypride small-animal PET recordings from 8 mice. *J Nucl Med.* 2010;51:1576–1583.
15. Dorr A, Sled JG, Kabani N. Three-dimensional cerebral vasculature of the CBA mouse brain: a magnetic resonance imaging and micro computed tomography study. *Neuroimage.* 2007;35:1409–1423.
16. Overhoff F, Brendel M, Jaworska A, et al. Automated spatial brain normalization and hindbrain white matter reference tissue give improved [^{18}F]-florbetaben PET quantitation in Alzheimer's model mice. *Front Neurosci.* 2016;10:45.
17. Sawiak SJ, Wood NI, Williams GB, Morton AJ, Carpenter TA. Voxel-based morphometry in the R6/2 transgenic mouse reveals differences between genotypes not seen with manual 2D morphometry. *Neurobiol Dis.* 2009;33:20–27.
18. Förster S, Grimmer T, Miederer I, et al. Regional expansion of hypometabolism in Alzheimer's disease follows amyloid deposition with temporal delay. *Biol Psychiatry.* 2012;71:792–797.
19. Liu B, Le KX, Park MA, et al. In vivo detection of age- and disease-related increases in neuroinflammation by ^{18}F-GE180 TSPO microPET imaging in wild-type and Alzheimer's transgenic mice. *J Neurosci.* 2015;35:15716–15730.
20. Hefendehl JK, Neher JJ, Suhs RB, Kohsaka S, Skodras A, Jucker M. Homeostatic and injury-induced microglia behavior in the aging brain. *Aging Cell.* 2014;13:60–69.
21. Cunningham CL, Martinez-Cerdeno V, Noctor SC. Microglia regulate the number of neural precursor cells in the developing cerebral cortex. *J Neurosci.* 2013;33:4216–4233.
22. Papadopoulos V, Baraldi M, Guilarte TR, et al. Translocator protein (18kDa): new nomenclature for the peripheral-type benzodiazepine receptor based on its structure and molecular function. *Trends Pharmacol Sci.* 2006;27:402–409.
23. Nimmerjahn A, Kirchhoff F, Helmchen F. Resting microglial cells are highly dynamic surveillants of brain parenchyma in vivo. *Science.* 2005;308:1314–1318.
24. Kalsbeek MJ, Mulder L, Yi CX. Microglia energy metabolism in metabolic disorder. *Mol Cell Endocrinol.* 2016;438:27–35.
25. Kai Kai MA, Pentreath VW. High resolution analysis of [^{3}H]2-deoxyglucose incorporation into neurons and glial cells in invertebrate ganglia: histological processing of nervous tissue for selective marking of glycogen. *J Neurocytol.* 1981;10:693–708.
26. Wolf SA, Boddeke HW, Kettenmann H. Microglia in physiology and disease. *Annu Rev Physiol.* 2017;79:619–643.
27. Ojo JO, Rezaie P, Gabbott PL, Stewart MG. Impact of age-related neuroglial cell responses on hippocampal deterioration. *Front Aging Neurosci.* 2015;7:57.
28. Matt SM, Johnson RW. Neuro-immune dysfunction during brain aging: new insights in microglial cell regulation. *Curr Opin Pharmacol.* 2016;26:96–101.
29. Gulyás B, Vas A, Toth M, et al. Age and disease related changes in the translocator protein (TSPO) system in the human brain: positron emission tomography measurements with [^{11}C]vinpocetine. *Neuroimage.* 2011;56:1111–1121.
30. Walker FR, Nilsson M, Jones K. Acute and chronic stress-induced disturbances of microglial plasticity, phenotype and function. *Curr Drug Targets.* 2013;14:1262–1276.
31. Aanerud J, Borghammer P, Chakravarty MM, et al. Brain energy metabolism and blood flow differences in healthy aging. *J Cereb Blood Flow Metab.* 2012;32:1177–1187.
32. Flurkey K, Currer J, Harrison D. *The Mouse in Aging Research.* Burlington, MA: American College Laboratory Animal Medicine (Elsevier); 2007.
33. Zimmer ER, Parent MJ, Souza DG, et al. [^{18}F]FDG PET signal is driven by astroglial glutamate transport. *Nat Neurosci.* 2017;20:393–395.
34. Edison P, Ahmed I, Fan Z, et al. Microglia, amyloid, and glucose metabolism in Parkinson's disease with and without dementia. *Neuropsychopharmacology.* 2013;38:938–949.
35. Xiong G, Paul C, Todica A, Hacker M, Bartenstein P, Boning G. Noninvasive image derived heart input function for CMRglc measurements in small animal slow infusion FDG PET studies. *Phys Med Biol.* 2012;57:8041–8059.
36. Backes H, Walberer M, Endepols H, et al. Whiskers area as extracerebral reference tissue for quantification of rat brain metabolism using ^{18}F-FDG PET: application to focal cerebral ischemia. *J Nucl Med.* 2011;52:1252–1260.
37. Dukart J, Mueller K, Horstmann A, et al. Differential effects of global and cerebellar normalization on detection and differentiation of dementia in FDG-PET studies. *Neuroimage.* 2010;49:1490–1495.